Catalysis Science & Technology

ROYAL SOCIETY OF CHEMISTRY

PAPER

View Article Online
View Journal

Cite this: DOI: 10.1039/d0cy01387k

Selective oxidation of crotyl alcohol by Au_xPd bimetallic pseudo-single-atom catalysts†

Brandon A. Chivers and Robert W. J. Scott *

AuPd bimetallic single-atom catalysts are being extensively studied as selective catalysts for hydrogenation and oxidation reactions due to their high selectivity. Previous work in our group has shown that alloy and core–shell AuPd nanoparticle catalysts can selectively oxidize crotyl alcohol to crotonaldehyde at room temperature in base-free conditions. In this work, we discuss the synthesis, extensive characterization, and activity for crotyl alcohol oxidation across a series of Au_xPd catalysts (x = 4, 3, 2, and 1) made by both co-reduction and sequential reduction strategies, in order to examine whether single-atom systems can lead to improved activity and/or selectivity for this reaction. X-ray absorption spectroscopy data shows that both co- and sequentially-reduced Au_4Pd catalysts have very small Pd–Pd coordination numbers, with values of 1.2 ± 0.3 and 1.6 ± 0.3, respectively, which indicates that they are closest to single-atom systems. The co-Au_4Pd catalyst, with the lowest Pd–Pd CN, also exhibits the highest selectivity for the selective oxidation of crotyl alcohol to crotonaldehyde. We were further able to enhance the selectivity of the AuPd nanoparticle catalysts by incorporating vinyl acetate as a hydride scavenger. We show in this paper that dispersing Pd in a Au matrix can lead to very selective catalysts while also lowering the amount of Pd needed in the system.

Received 9th July 2020,
Accepted 18th September 2020

DOI: 10.1039/d0cy01387k

rsc.li/catalysis

Introduction

Metallic nanomaterials such as metal nanoparticles (NPs) and nanoclusters (NCs) are well-known materials in the catalysis field for catalyzing numerous reactions such as oxidation,[1–6] hydrogenation,[7–12] and C–C coupling[13–15] reactions. Recently, there has been a great deal of research on single-atom catalysts (SACs), in which catalytic metal atoms are singly isolated within a matrix of another metal or on a support material.[9,12,16–29] Common metals that are used to synthesize SACs include Pt,[30–33] Au,[34] Ir,[35] Rh,[36] Pd,[8,25,37–39] Fe,[40,41] and Co,[42] with Pd and Pt being used most frequently. The intrigue behind SACs is due to their ability to catalyze numerous reactions with high selectivity while using a much lower metal loading relative to their NP and NC counterparts.[8,16–18,21,43–46] In the case of SACs, each metal atom is theoretically contributing to the reaction. In contrast, sub-surface metal atoms in NPs and NCs can be unused throughout a catalytic cycle.[16,17] Not only has there been catalytic improvements shown with SACs, but also economic benefits as the cost of making such catalysts can be much lower because less metal is needed. Thorough characterization processes are required to determine whether a SAC has atomic dispersion of metal on a support surface. Conventional techniques include TEM techniques such as high-angle annular dark-field (HAADF) imaging or high-resolution transmission electron microscopy (HR-TEM).[27,37,38,47] Perhaps the most powerful characterization tool is the use of synchrotron radiation, where techniques such as X-ray absorption spectroscopy (XAS) can be used to determine local atomic information on a metal center in a catalyst.[48–50] Through fitting of the EXAFS region, valuable information such as coordination numbers and bond distances can be determined for a metal center of interest, which allows one to piece together the atomic structure of a catalyst.[16,24,33,38,49,51–58]

The selective oxidation of alcohols has been studied extensively by our group and others using monometallic Au and Pd catalysts, as well as bimetallic AuPd catalysts with varying metal loadings and catalyst sizes.[4,23,24,44,45,51,52,59–71] Pd is a powerful metal catalyst for oxidation and hydrogenation reactions, while Au contributes to bolster the performance of Pd through synergistic electronic effects.[4,8–10,12,44,51–53,72–78] We have previously shown that bimetallic PVP-stabilized AuPd NP catalysts are more active and selective for alcohol oxidation reactions than their monometallic Pd and Au NP counterparts. Additionally, Balcha *et al.*[24] showed that the selective oxidation of allylic alcohols such as crotyl alcohol could be carried out at room temperature (25 °C) and base-free conditions, and that the most effective catalysts were sequentially reduced systems that had approximate core–shell structures and Au : Pd ratios of 1 : 3. Similarly, Abis *et al.*[60] recently synthesized an $AuPd/TiO_2$

Department of Chemistry, University of Saskatchewan, 110 Science Place, Saskatoon, Saskatchewan, S7N 5C9, Canada. E-mail: robert.scott@usask.ca

† Electronic supplementary information (ESI) available: Fitted EXAFS spectra in *R*-space. See DOI: 10.1039/d0cy01387k

catalyst for the plasmonic oxidation of glycerol at 90 °C under base-free conditions, with a maximum activity was seen at an Au : Pd ratio of 2 : 1. Thus, while it has been shown that AuPd systems are excellent selective oxidation catalysts under various reaction conditions, we wish to see if selectivity can be enhanced by completely dispersing the Pd in the Au matrix.

SACs are becoming more prominent in the catalysis field, with numerous reports of SACs being used for oxidation, hydrogenation, and C–C coupling reactions.[5,8,10,29,32,38,40,41,44,79–84] AuPd SAC systems have been studied for selective hydrogenation catalysts, due to the high activity of Pd for such reactions.[8,28,45,59,85,86] Liu *et al.*[8] designed an AuPd SAC for the selective hydrogenation of 1-hexyne to 1-hexene and showed an improvement in the selectivity of an AuPd SAC compared to a Pd NP catalyst under room temperature (25 °C) conditions. While there are countless examples of AuPd nanoparticle systems catalyzing selective oxidation reactions, very few examples exist employing bimetallic AuPd SACs.[44,45] Recently, Zhu *et al.*[45] successfully synthesized a collection of dilute AuPd nanoalloys with varying Au : Pd atomic ratios which were thoroughly characterized *via* TEM imaging and XAS to evaluate the atomic structure of the nanoalloys. The catalytic activity was evaluated for the oxidation of benzyl alcohol at 90 °C in the absence of a base, and it was determined that the Au : Pd catalyst with a 1 : 1 ratio showed the highest activity and selectivity for the oxidation reaction.

Herein, we report the synthesis of co-reduced and sequentially-reduced Au_xPd catalysts with varying Au : Pd ratios (x = 4, 3, 2, and 1), and characterize them by TEM and XAS. For the Au_4Pd catalysts, EXAFS modelling shows that Pd is in a pseudo-single-atom coordination environment in the Au NP matrix. The Au_xPd catalysts are then evaluated for the selective oxidation of crotyl alcohol; results from these selective oxidation reactions show that the pseudo-single-atom catalyst (co-Au_4Pd) exhibits the highest activity and selectivity towards crotonaldehyde. We also show that one can further enhance the selectivity through the addition of a sacrificial alkene, vinyl acetate, to the system.

Experimental

Materials

Potassium tetrachloropalladate(II) (K_2PdCl_4, 98%, Sigma-Aldrich), gold(III) chloride trihydrate ($HAuCl_4{\cdot}3H_2O$, ≥99.9% trace metal basis, Sigma-Aldrich), polyvinylpyrrolidone (PVP, M.W. 58 000, Alfa Aesar), sodium borohydride ($NaBH_4$, 98%, Sigma-Aldrich), L-ascorbic acid ($C_6H_8O_6$, reagent grade, crystalline, Sigma-Aldrich), aluminum oxide (Al_2O_3, pore size 58 Å, ~150 mesh, Sigma-Aldrich), crotyl alcohol (CH_3-$CH{=}CHCH_2OH$, mixture of *cis* and *trans*, Sigma-Aldrich), vinyl acetate (VA, $C_4H_6O_2$, stabilized for synthesis, Sigma-Aldrich), acetone (Certified ACS, ≥99.5%, Fisher), methanol (CH_3OH, Certified ACS, ≥99.8%, Fisher), and ethyl acetate ($CH_3COOC_2H_5$, ACS reagent, ≥99.5%, Sigma-Aldrich) were used as received. Milli-Q (Millipore, Bedford, MA) deionized water (18 MΩ cm) was used throughout.

Co-reduction synthesis of Au_xPd catalysts

Co-reduced Au_xPd (x = 4, 3, 2, and 1) nanoparticles (NPs) were synthesized by modifying procedures from Tsunoyama *et al.*,[87] and Balcha *et al.*[24] 1.0 g PVP (MW ~ 58 000) was dissolved in 5.8 mL H_2O in a 100 mL round-bottom flask at room temperature (22 °C). The solution was then placed in an ice-bath and cooled to 0 °C. To this cooled solution, 6.2 mL K_2PdCl_4 (9.0×10^{-5} mol Pd) and 1, 2, 3, or 4 equiv. of $HAuCl_4{\cdot}3H_2O$ (9.0×10^{-5} mol Au to 3.6×10^{-4} mol Au) was added depending on the desired ratio of Pd/Au. In a separate 100 mL round-bottom flask, 1.0 g PVP (MW ~ 58 000) was dissolved in 6.0 mL H_2O and cooled to 0 °C in an ice bath. After 20 minutes of stirring, 2.0 mL of ice-cold $NaBH_4$ (5 equiv. to the amount of Au) was added, followed by stirring for another 10 minutes. The stirring speed was increased to 1600 rpm, and the reducing agent solution was added to solution containing the metal salt as quickly as possible. The final solution changed from a yellow–brown solution to a dark brown–black solution immediately after the solutions were mixed. This dark solution was then stirred for 30 minutes in an ice bath, followed by stirring at 30 minutes at room temperature (22 °C). Once the stirring was completed, the catalyst solution was placed in cellulose dialysis membranes with a molecular weight cutoff of 12 000 g mol^{-1} and dialyzed for 24 hours in 500 mL of deionized water without stirring. A final [Pd] of 3.0 mM was achieved, with the final [Au] = 3.0 mM, 6.0 mM, 9.0 mM, and 12 mM depending on the Pd/Au ratio.

Sequential reduction synthesis of core–shell Au_xPd catalysts

Sequentially-reduced core–shell Au_xPd (x = 4, 3, 2, and 1) NPs were synthesized with slight modifications of literature protocols.[52] First, an Au NP seed solution was synthesized ([Au] = 18.2 mM), and then K_2PdCl_4 was reduced using ascorbic acid in the Au NP solution to give sequentially-reduced Au_xPd.

Au NPs were synthesized as follows: 2.0 g PVP (MW ~ 58 000) was dissolved in a mixture of water/methanol (15 mL/16 mL) in a 100 mL round bottom flask. The flask was placed in an ice bath and cooled to 0 °C before the addition of 473 mg $HAuCl_4{\cdot}3H_2O$ (6.0×10^{-4} mol Au). In another 100 mL round bottom flask, 1.0 g PVP (MW ~ 58 000) was dissolved in a water/methanol mixture (3 mL/3 mL), placed in an ice bath and cooled to 0 °C. After 20 minutes, 2.0 mL of ice-cold $NaBH_4$ (7 equiv. to Au) was added and stirred for a further 10 minutes. The stirring speed was increased to 1600 rpm, and the solution containing the reducing agent was added to the flask containing the Au salt as quickly as possible. The solution changed from a yellow solution to a dark red solution upon $NaBH_4$ addition. This solution was left to stir in an ice bath for 30 minutes, following by stirring at room temperature (22 °C) for 30 minutes. The dark red solution of Au NPs was then dialyzed as detailed earlier. After dialysis, the Au NP solution was concentrated by removing methanol to give an aqueous solution with a final [Au] of 18.2 mM. The

methanol was removed by stirring the post-dialysis solution at 1200 rpm and heating it in a water bath to 40 °C under high vacuum conditions.

Sequentially-reduced Au_xPd NPs were synthesized by mixing 1.0 g PVP (MW ~ 58 000) with 9.0×10^{-5} mol Pd (K_2PdCl_4) and 18.2 mM Au NPs so that the Au ratio to Pd was 1 : 1, 2 : 1, 3 : 1, or 4 : 1 (9.0×10^{-5} mol Au to 3.6×10^{-4} mol Au). This mixture was stirred at 800 rpm and cooled in an ice bath to 0 °C for 5 minutes before increasing the stir rate to 1600 rpm and adding 10 equiv. of ascorbic acid (equiv. with respect to the moles of Pd, 159 mg, 9.0×10^{-4} mol ascorbic acid) to reduce the Pd. The solution colour slowly changed from dark red to black after stirring the solution in ice at 1400 rpm for 1 hour. After all reactants were added, the final volume of the solution was adjusted to be 30.0 mL. The solution was dialyzed overnight using similar dialysis procedures as noted above. The final solution had a [Pd] = 3.0 mM, with the [Au] = 3.0 mM, 6.0 mM, 9.0 mM, and 12 mM depending on the Pd/Au ratio.

Characterization

UV-vis spectra were obtained using a Varian Cary 50 Bio UV-visible spectrophotometer with a scan range of 200–1000 nm and an optical path length of 1.0 cm. Transmission electron micrographs (TEM) were taken with an HT7700 TEM operating at 100 kV. TEM grids were prepared by placing a few drops of catalyst in Milli-Q deionized water onto a lacey carbon TEM grid (Electron Microscopy Sciences). Particle sizes were measured using the software ImageJ by measuring at least 70 particles for each sample.[88] All X-ray photoelectron spectroscopy (XPS) measurements were collected using a Kratos (Manchester, UK) AXIS Supra system at the Saskatchewan Structural Sciences Centre (SSSC). This system is equipped with a 500 mm Rowland circle monochromated Al Kα (1486.6 eV) source and combined hemispherical analyzer (HSA) and spherical mirror analyzer (SMA). A spot size of hybrid slot (300 × 700 microns) was used. All survey scan spectra were collected in the −5–1200 eV binding energy range in 1 eV steps with a pass energy of 160 eV. High-resolution scans of 2 regions were also conducted using 0.05 eV steps with a pass energy of 20 eV. An accelerating voltage of 15 keV and an emission current of 10 mA was used for the analysis. The XPS spectra were analyzed using the CasaXPS software program.[89] High-resolution scans were obtained for Pd 3d and Au 4f peaks, which were then calibrated to a C 1s peak at 284.8 eV.

The hard X-ray microanalysis beamline (HXMA) 061D-1 (energy range, 5–30 keV; resolution, 1×10^{-4} $\Delta E/E$) and biological X-ray absorption spectroscopy beamline (BioXAS) 07ID-2M (energy range, 5–32 keV; resolution, 5×10^{-5} $\Delta E/E$) at the Canadian Light Source (CLS) were used for collecting X-ray absorption spectra (XANES and EXAFS) at the Pd K-edge and Au L_{III}-edge. The energy scan range for measurements on both beamlines was between −200 eV to +800 eV at each edge. Pd and Au foils were used for references at the Pd K-edge and Au L_{III}-edge, respectively. All measurements were conducted in both transmission and fluorescence modes at room temperature (22 °C), with Au_xPd samples loaded onto alumina at 2.0% by weight Pd (Au weight percentage varied with Pd/Au ratio) using an acetone precipitation method.[90] These solid powders were placed into a Teflon sample holder and sealed with Kapton tape. XANES and EXAFS data analysis was performed using the software package IFEFFIT.[91] fcc bulk lattice parameters (*i.e.*, first shell coordination numbers of 12) were used to fit the Pd and Au reference foil data and determine the amplitude reduction factor (S_o^2) for both foils. For the Au foil, S_o^2 was determined to be 0.90 and 0.88 on BioXAS and HXMA beamlines, respectively. For the Pd foil, S_o^2 was determined to be 0.82 on both BioXAS and HXMA. These S_o^2 values were fixed and used to determine the EXAFS parameters for all samples. The soft X-ray microcharacterization beamline (SXRMB) 06B1-1 (energy range, 1.7–10 keV; resolution, 1.0×10^4 $\Delta E/E$) at the CLS was used for collecting XANES spectra at the Pd L_{III}-edge. SXRMB samples were prepared in two ways. Solid samples were loaded onto double-sided tape, and fluorescence data was collected under a helium atmosphere. Liquid samples were analyzed by loading solution into SPEX CertiPrep Disposable XRF X-Cell sample cups and covering the cup with a 4 μm ultralene window film. Data was collected in fluorescence mode.

Catalytic oxidation of crotyl alcohol

The oxidation of crotyl alcohol was performed following previous literature protocols as detailed in Maclennan *et al.*[51] Co- and sequentially-reduced Au_xPd samples, with [Pd] = 3.0 mM and varying [Au] depending on the Pd/Au ratio, were studied in this catalytic oxidation reaction. To a 50 mL 3-neck round-bottom flask, 5.0 mL of the catalyst solution was added. A condenser was then attached to the middle neck of the flask and the other two necks covered with septa. A needle was connected to one end of the flask and the tip placed into the catalyst solution in order to sparge the solution with $O_{2(g)}$ during the reaction. The system was purged with $O_{2(g)}$ for 20 minutes before adding 250 equiv. of crotyl alcohol (0.32 mL, for a substrate : Pd ratio of 250 : 1) *via* a syringe needle. The reaction was then stirred at 1400 rpm for 3 hours at 22 °C. After the 3 hour reaction, 2.0 mL of the reaction mixture was collected in a vial and transferred to 2.0 mL of ethyl acetate. This was done by mixing the reaction mixture with ethyl acetate (1.0 mL per extraction) by shaking it vigorously in a vial, and then the contents were transferred to two 2.0 mL centrifugation tubes and centrifuged at 6000 rpm for 10 seconds. The top layer of the neat extract was collected for analysis, while the bottom water/catalyst layer was discarded. Conversion, selectivity, and turnover numbers for the reaction were obtained from gas chromatography (GC) using an FID detector (Agilent Technologies 7890A) and an HP-Innowax capillary column.

The ethyl acetate extract was used for GC–FID analysis. Two reactions were run for each Au_xPd sample with three injections per reaction.

The oxidation of crotyl alcohol was also performed in the absence of $O_{2(g)}$, using vinyl acetate as a sacrificial alkane.[92] For this reaction, 5.0 mL of the Au_xPd catalyst solution was delivered into a 100 mL round-bottom flask. 0.35 mL of vinyl acetate was then added, and the mixture stirred at 1400 rpm. After 2 minutes of stirring, 0.32 mL of crotyl alcohol was added (1 : 1 vinyl acetate : crotyl alcohol ratio), and the reaction was continued for 3 hours before GC–FID analysis. Product extraction was performed in the same way previously mentioned. GC–FID calibration curves were run for this reaction using the starting substrate crotyl alcohol, and the three main products crotonaldehyde, 1-butanol, and 3-buten-1-ol. Six different concentrations were run for each reactant, with three injections performed at each concentration. Linear calibration curves were obtained for all species with R^2 values of ~0.99 for all systems.

Results and discussion

Synthesis and characterization of co- and sequentially-reduced Au_xPd catalysts

The concentration of Pd was kept constant for the crotyl alcohol oxidation reactions at 3.0 mM. This value was chosen with the idea of evaluating these catalysts with XAS measurements. In order to obtain high-quality XAS data that exhibits a deep *k*-space, a higher concentration of metals needed to be used. Therefore, the concentration of Pd was 3.0 mM, while the [Au] increased from 3.0 mM to 12 mM, depending on the Au : Pd ratio. Since a high metal concentration was used, the size of these catalysts was monitored by TEM to ensure that particle agglomeration and growth did not occur, while retaining relatively monodisperse particle sizes. Both co-reduction and sequential reduction strategies were used to obtain Au_xPd catalysts. The co-reduced (co-) Au_xPd catalysts were made by reducing an Au and Pd precursor in the presence of a stabilizer, while sequentially-reduced (seq-) Au_xPd catalysts were made by first reducing an Au precursor to give Au NPs, then reducing a Pd precursor into the Au NP matrix. Fig. 1 shows TEM images for each ratio of co- and seq-Au_xPd catalysts. A complete table of average particle sizes and standard deviations are listed in Table 1.[88]

For the co-Au_xPd catalysts, particle sizes vary between 3.0 and 3.6 nm. For the seq-Au_xPd catalysts, particle sizes vary between 3.6 and 4.9 nm. The particle sizes of each catalyst for both reduction methods are all within similar ranges, which would suggest that particle growth or agglomeration is not occurring, meaning these catalysts are stable under the reduction conditions during their synthesis. Smaller NP catalysts ensure that the surface of the catalyst can be better studied using XAS, as a larger fraction of atoms is on the surface of the NPs.

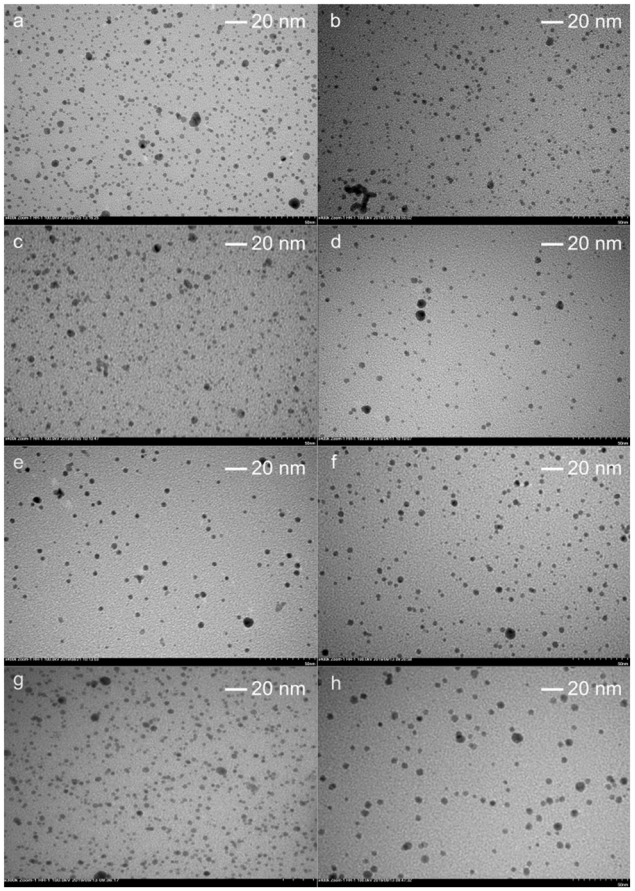

Fig. 1 TEM images of a) co-Au_4Pd, b) co-Au_3Pd, c) co-Au_2Pd, d) co-AuPd, e) seq-Au_4Pd, f) seq-Au_3Pd, g) seq-Au_2Pd, and h) seq-AuPd catalysts.

From Table 1, the average particle size for the Au NP seed solution is 3.6 ± 1.1 nm. As Pd is added into the system, the seq-Au_xPd particle sizes increase as the ratio of Au : Pd is decreased towards unity (*i.e.*, 1 : 1). Expected particle sizes can be calculated for the seq-Au_xPd catalysts using eqn (1):[93]

$$D = D_{\text{core}}\left(1 + \frac{V_{\text{Pd}}[\text{Pd}]}{V_{\text{Au}}[\text{Au}]}\right)^{\frac{1}{3}} \quad (1)$$

where D_{core} is the particle size of the Au NPs, V_{Pd} is the molar volume of Pd, [Pd] is the concentration of Pd, V_{Au} is the

Table 1 Average TEM particle sizes

Catalyst	Particle size (nm)
co-Au_4Pd	3.1 ± 0.9
co-Au_3Pd	3.0 ± 1.1
co-Au_2Pd	3.6 ± 1.0
co-AuPd	3.5 ± 1.3
seq-Au_4Pd	3.6 ± 0.9
seq-Au_3Pd	3.7 ± 0.8
seq-Au_2Pd	4.0 ± 1.0
seq-AuPd	4.9 ± 1.3
Au NPs	3.6 ± 1.1

molar volume of Au, and [Au] is the concentration of Au. For the seq-Au$_x$Pd catalysts, particle sizes of 3.8, 3.9, 4.1, and 4.4 nm were predicted for Au : Pd ratios of 4 : 1, 3 : 1, 2 : 1, and 1 : 1, respectively. These values correspond well with the measured particle sizes in Table 1.

To investigate whether secondary nucleation of Pd is occurring in the sequentially reduced system, a histogram of particle sizes is shown in Fig. 2. Histograms were generated by plotting the raw count of binned particle sizes for each sequentially-reduced catalyst and Au NPs and then fitting normal distribution curves to the raw data. The highest count of particle sizes occurs between 3–5 nm for each system, including the Au NPs. As Pd is introduced into the system (*i.e.*, to form seq-Au$_x$Pd), a new distribution of smaller particle sizes is not observed. This would indicate that a secondary nucleation event of new Pd NPs is not occurring, suggesting the system is bimetallic, though the catalysts are characterized further below to show they are indeed bimetallic.

Fig. 3 contains UV-vis spectra comparing Au NP seeds with the bimetallic Au$_4$Pd NP system after Pd is deposited on the surface, as well as the co-reduced Au$_4$Pd NP system. A typical absorption peak is seen ~550 nm for Au NPs which is caused by surface plasmon resonance.[94] In the case of co-Au$_4$Pd, no SPR peak is seen in the system. This would point towards Au–Pd interactions becoming more prominent, and a bimetallic alloy structure for the NPs.[24] On the other hand, for the seq-Au$_4$Pd catalyst, a slight peak can be seen at ~520 nm after the Pd reduction, which is dampened and shifted to lower energy compared to the pure Au NP plasmon peak. This indicates that Au–Au interactions are still prevalent in the system, though a dampening of the peak is consistent with the addition of Pd on the surface of Au.[24,68,93]

XPS studies were performed to characterize the surface composition of both co- and sequentially-reduced Au$_4$Pd catalysts. Fig. 4 shows XPS spectra for both co- and seq-Au$_4$Pd samples. In Fig. 4a, Pd 3d$_{5/2}$ and 3d$_{3/2}$ peaks were fit for co-Au$_4$Pd, giving binding energies of 334.6 and 339.9 eV, respectively. These values correlate reasonably well with literature to metallic Pd(0) at 335.1 eV and 340.4,

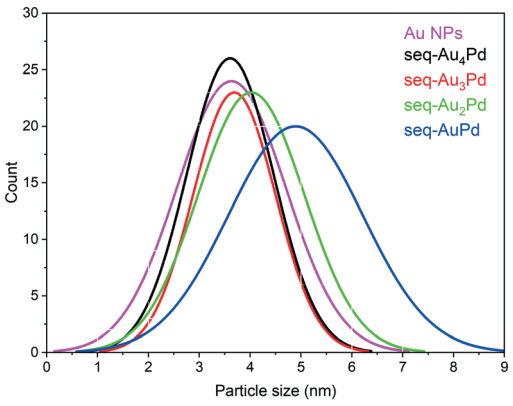

Fig. 2 Distribution of particle sizes measured for Au NPs and all seq-Au$_x$Pd catalysts.

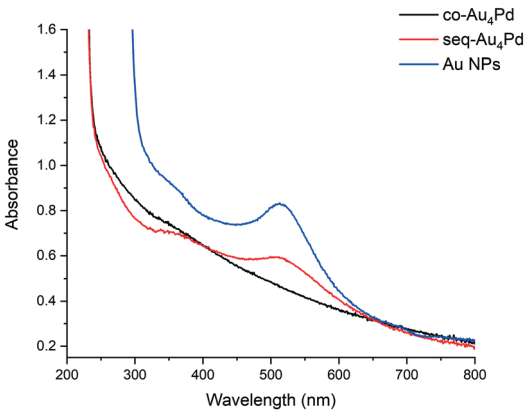

Fig. 3 Comparison of UV-vis spectra for co-Au$_4$Pd, seq-Au$_4$Pd, and Au NPs.

respectively.[95] Fig. 4b shows Au 4f$_{7/2}$ and 4f$_{5/2}$ peaks for co-Au$_4$Pd, with binding energies of 82.8 and 86.4 eV, respectively. These values also correlate well with metallic Au(0) in the literature at 83.2 and 86.9 eV, respectively.[96] Fig. 4c shows seq-Au$_4$Pd fitted peaks for Pd 3d$_{5/2}$ and 3d$_{3/2}$ with binding energies of 334.6 and 339.9 eV, respectively. Again, these values correlate well to Pd(0) from the literature.[95] Lastly, Fig. 4d shows seq-Au$_4$Pd fitted peaks for Au 4f$_{7/2}$ and 4f$_{5/2}$ with binding energies of 83.0 and 86.6 eV, respectively. These values correlate well with the previously mentioned literature.[96] From this analysis, it can be concluded that both Au and Pd are in their metallic forms on the surface of the catalyst, meaning a full reduction has occurred. The surface analysis also confirms that both metallic Au and Pd are present in the system, though more in-depth results from X-ray absorption spectroscopy (XAS) will be discussed below to provide further conclusions on the make-up of these catalysts at each Au : Pd ratio.

Fig. 5 contains XANES data at the Pd L$_{III}$-edge, showing a reference Pd foil compared to each ratio of co-Au$_x$Pd

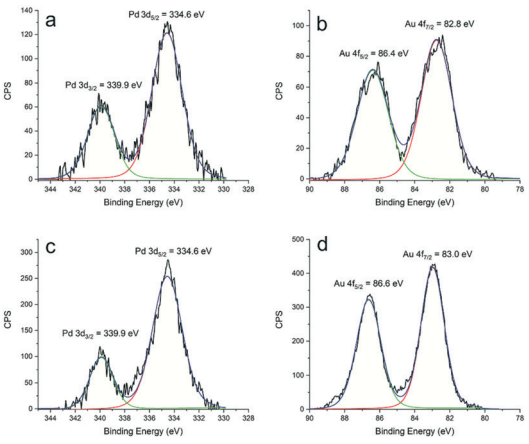

Fig. 4 Fitted XPS spectra for (a) co-red Au$_4$Pd Pd 3d peak, (b) co-red Au$_4$Pd Au 4f peak, (c) seq-Au$_4$Pd Pd 3d peak, and (d) seq-Au$_4$Pd Au 4f peak.

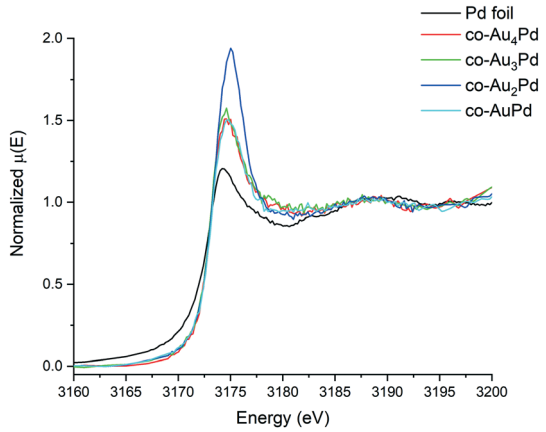

Fig. 5 Pd L_{III}-edge XANES data of co-Au_xPd samples.

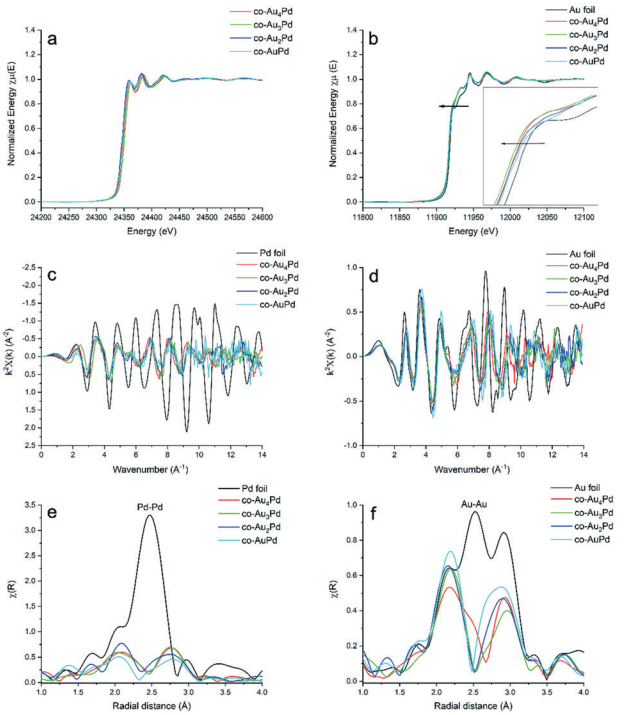

Fig. 6 X-ray absorption spectroscopy data for co-Au_xPd catalysts. (a) Pd K-edge XANES, (b) Au L_{III}-edge XANES, (c) Pd K-edge *k*-space, (d) Au L_{III}-edge *k*-space, (e) Pd K-edge *R*-space, and (f) Au L_{III}-edge *R*-space.

catalysts. The white-line feature at 3173 eV is caused by the excitation of electrons from the $2p^{3/2}$ to 4d band in Pd.[61,97] The increase in white line intensity relative to Pd foil would suggest for each co-Au_xPd catalyst that electrons are being withdrawn from the 4d band of Pd by Au in the catalyst.[51,98,99] Also, a shift in the energy of the white line is observed for co-Au_xPd catalysts, further concluding that electrons are being withdrawn from the 4d band of Pd by Au. This allows one to conclude that our catalyst is a bimetallic AuPd system as these apparent shifts in white line intensity and energy correlate well with the literature from our group and others.[51,61,98,99] We are uncertain as to why the co-Au_2Pd system showed the most electron-deficient Pd.

The bimetallic nature of both co- and sequentially-reduced Au_xPd catalysts was evaluated *via* XAS. Fig. 6 contains XAS data collected for co-Au_xPd catalysts at each ratio of Au : Pd (*i.e.*, 4 : 1, 3 : 1, 2 : 1, and 1 : 1). Fig. 6a shows XANES spectra from the Pd K-edge for each co-Au_xPd catalyst. The Pd K-edge measures the transition from a 1s orbital to 5p orbital in Pd at the edge, with a white line observed near 24 350 eV. Fig. 6b shows XANES spectra from the Au L_{III}-edge for each co-Au_xPd catalyst. A shift to lower white line energy for the bimetallic samples relative to the Au foil would indicate an increase in electron density of the 5d band of Au.[24,98,100] This result, combined with results discussed from Fig. 5, shows that Au is withdrawing electrons from Pd, increasing the electron density of the Au 5d band and depleting electrons from the 4d band of Pd. Fig. 6c and d contain *k*-space data collected on the Pd K-edge and Au L_{III}-edge, respectively, for all co-Au_x-Pd catalysts. A comparison between the bimetallic samples and monometallic reference foils shows an obvious shift in periodicity at both metal edges beyond a wavenumber of 4 $Å^{-1}$. This indicates there is a strong Au–Pd interaction in the co-Au_xPd catalysts, providing further proof that they are bimetallic.[56] The *R*-space data at the Pd K-edge and Au L_{III}-edge for co-Au_xPd catalysts are shown in Fig. 6e and f. More intense peaks correlate to larger M–M coordination numbers for the metal center being analyzed. In Fig. 6e, the sharp peak seen slightly below 2.5 Å for the Pd reference foil is due to first shell Pd–Pd interactions, while significantly reduced Pd–M peak intensities are seen for the co-Au_xPd catalysts. Fitted EXAFS spectra which are phase-corrected for both the Pd–Pd peak and Au–Au peak are included in the ESI.† Fig. 6e suggests that a minute Pd–M interaction is observed for the co-reduced systems, indicating that Pd is likely located on the surface of Au. To quantitatively show this, a further discussion on the fitting of this data will be included later in this section. Fig. 6f shows the *R*-space data at the Au L_{III}-edge for all co-reduced Au_xPd catalysts as well as Au foil. A strong first shell Au–Au interaction is seen slightly above 2.5 Å, while a strong Au–Pd interaction is observed slightly below 2.25 Å for each co-Au_xPd sample. This strong Au–Pd interaction in the co-Au_xPd catalysts suggests that these systems are alloys. There is a qualitative shift in the co-reduced spectra *versus* the Au foil, further providing proof of strong Au–Pd interactions.

Fig. 7 shows the XANES region at the Pd L_{III}-edge for sequentially-reduced catalysts, where an increase in white line intensity at 3173 eV, as well as a shift in white line energy is observed. As discussed for the co-reduced system, an increase in white line intensity and shift to higher energy indicates electron withdrawal from the 4d band of Pd, though the shift is less dramatic for the seq-Au_xPd system. Overall the higher white line intensity of the seq-Au_xPd samples, as compared to the co-Au_xPd samples, suggests that Pd has reduced 4d occupancy in the seq-Au_xPd system. This may be due to more of the Pd being on the surface in this system.

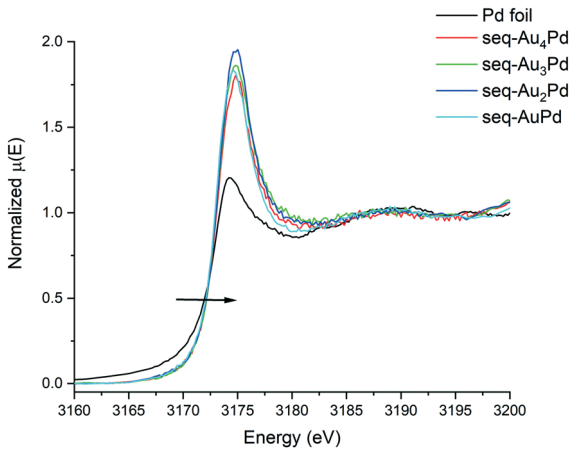

Fig. 7 Pd L_{III}-edge XANES data for seq-Au_xPd samples.

Fig. 8 contains XANES and EXAFS spectra for seq-Au_xPd catalysts at each ratio of Au : Pd (*i.e.*, 4 : 1, 3 : 1, 2 : 1, and 1 : 1). Fig. 8a shows XANES spectra from the Pd K-edge for all seq-Au_xPd catalysts. As previously mentioned, this is the transition from a 1s to 5p orbital for Pd, with a white line observed near 24 350 eV. The spectra closely resemble that of Pd foil at the edge suggesting that Pd is reduced in all the samples, though the dampened EXAFS region suggests much lower coordination numbers for Pd in the bimetallic NPs. Fig. 8b shows the Au L_{III}-edge XANES data for each seq-Au_xPd sample. No obvious shift in the white line is observed, indicating that an increase in electron density in the 5d band of Au is not as prominent for these samples. This is likely because most Au is not in direct contact with Pd in these samples (as is shown below). Fig. 8c and d show the *k*-space data collected on both metal edges for the seq-Au_xPd catalysts. No significant shifts in the periodicity of the wave are observed at either metal edge, though the amplitude of the wave at the Au L_{III}-edge correlates well with the Au reference foil, indicating that Au is in a near-bulk coordination environment. Again, this will be discussed in more detail later, though a suggestion can be made that the seq-Au_xPd catalysts take on a core–shell morphology.[24] Fig. 8e contains *R*-space data for each seq-Au_xPd catalyst at the Pd K-edge as well as a Pd reference foil. Like the co-reduced catalysts, an intense feature just below 2.5 Å is observed for the reference foil, though weak Pd–M interactions are observed for the seq-Au_xPd catalyst. There is a slight qualitative difference in peak shapes between the co- and seq-Au_xPd catalysts, which will be discussed in more detail below. Fig. 8f shows the *R*-space data collected on the Au L_{III}-edge for each seq-Au_xPd catalyst and an Au reference foil. A strong Au–Au interaction is observed for the Au reference foil as well as the seq-Au_xPd catalysts just above 2.5 Å, indicating a near-bulk Au environment in the seq-Au_xPd catalysts.

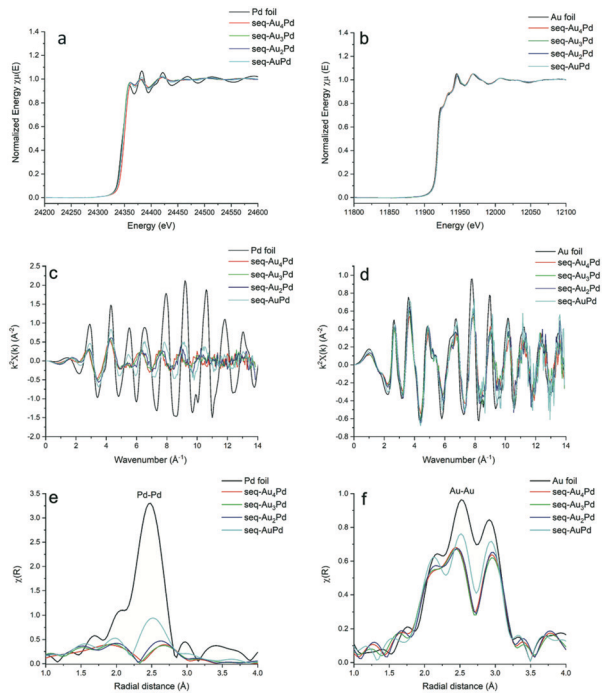

Fig. 8 X-ray absorption spectroscopy data for seq-Au_xPd catalysts. (a) Pd K-edge XANES, (b) Au L_{III}-edge XANES, (c) Pd K-edge *k*-space, (d) Au L_{III}-edge *k*-space, (e) Pd K-edge *R*-space, and (f) Au L_{III}-edge *R*-space.

Fig. 9 provides an in-depth comparison of the Pd K-edge and Au L_{III}-edge between both co- and seq-Au_xPd catalysts at 4 : 1 and 1 : 1 Au : Pd ratios. In Fig. 9a, *R*-space data at the Pd K-edge is shown for co- and seq-Au_xPd samples. As mentioned previously, the reduction in amplitude for the Pd–Pd just below 2.5 Å indicates that most of the Pd is on the surface of both catalysts. The low intensity of the Pd–Pd peak may indicate low coordination numbers (CNs) for the Pd–Pd bond in both catalysts, though the data must be fit to quantify this Pd–Pd interaction in terms of CNs. Small features can be seen slightly shifted to a higher radial distance for both catalysts, indicating Au–Pd bonding. A slightly further shift is seen for co-Au_4Pd and co-AuPd relative to the seq-Au_xPd catalysts, indicating that Pd may be in more of an isolated environment compared to the seq-Au_xPd catalysts and Pd–Pd CNs are lower for each ratio of Au : Pd, though further quantification was done through fitting the EXAFS data. Fig. 9b contains the Au L_{III}-edge *R*-space data for co- and sequentially-reduced Au_xPd catalysts at the same ratios. Qualitatively, there are nuanced differences in line shapes between the co- and seq-Au_xPd

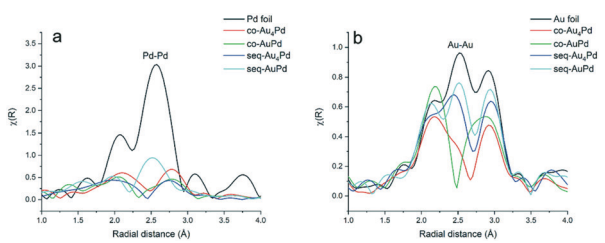

Fig. 9 *R*-Space data comparing co-Au_xPd and seq-Au_xPd catalysts at (a) Pd K-edge and (b) Au L_{III}-edge.

catalysts. The co-Au_xPd catalysts show a stronger Au–Pd interaction just below 2.25 Å than the seq-Au_xPd catalysts, indicating more Au–Pd mixing in the co-reduced catalysts. A more significant difference in the *R*-space data between co- and seq-Au_xPd is seen as the seq-Au_xPd takes on a very similar shape to the Au foil. This would qualitatively suggest that Au is in a near-bulk environment in the seq-Au_xPd catalyst with very strong Au–Au interactions, whereas a strong Au–Au interaction is not as prevalent in co-Au_xPd catalysts. Further quantitative conclusions can be made in regard to Pd–M and Au–M interactions by modelling CNs for Pd–Pd, Pd–Au, Au–Au, and Au–Pd interactions through EXAFS data fitting using the IFEFFIT software package.

Simultaneous EXAFS fitting of both the Pd K-edge and Au L_{III} edge was done using AuPd alloy fcc models, and fitting results are shown in Tables 2 and 3. In Tables 2 and 3, the element that comes first symbolizes the absorbing atom, while the second element symbolizes the neighbouring atom that scatters photoelectrons released by the absorbing atom (*e.g.* a PdAu interaction is a Pd absorbing atom with neighbouring first shell Au atoms). Both first shell Pd–Pd and Pd–Au interactions were quantified for all the co-reduced systems. For the Au_4Pd co-reduced NPs, the small CN of 1.2 ± 0.3 for the Pd–Pd interaction, along with a significant CN of 8.7 ± 0.8 for the Pd–Au interaction indicates that the Pd is nearly in a single-atom environment (*i.e.* a pseudo-single-atom-catalyst).[44,101] The co-reduced systems showed a slightly increased Pd–Pd CN of 2.5 ± 0.6, 2.5 ± 0.4, and 2.4 ± 1.2, for 3 : 1, 2 : 1, and 1 : 1 Au : Pd systems, respectively. This small increase in Pd–Pd CN signals that Pd is associated with neighbouring Pd atoms more often within the core or on the surface of Au. Notably, the Pd–Au CN begins to decrease with the Au : Pd ratio, going from 7.2 ± 0.9 down to 6.0 ± 2.4 for the 3 : 1 and 1 : 1 samples, respectively. Au–Au and Au–Pd first shell interactions were also quantified for all the co-reduced catalysts. A large CN of 7.1 ± 0.7 for the first shell Au–Au in the co-Au_4Pd catalyst was seen, indicating a large number of Au–Au neighbours. A low CN for Au–Pd in the co-Au_4Pd catalyst of 1.2 ± 0.3 was also quantified. As the ratio of Au : Pd decreases from 4 : 1 to 1 : 1, the CN of Au–Au decreases while the CN of Au–Pd increases. At an Au : Pd ratio of 1 : 1, the CN for Au–Au is 5.8 ± 0.9, and for Au–Pd is 3.7 ± 0.6. To conclude, the nearest catalyst to a SAC is the co-Au_4Pd system, with all other ratios showing a trend towards AuPd catalysts with more contiguous Pd domains (*i.e.*, higher coordination between Pd atoms). The total Pd–M and Au–M CNs can be calculated by adding together Pd–Au with Pd–Pd, and Au–Pd with Au–Au, respectively, to confirm which metal is preferentially on the surface of the catalysts. As the ratio of Au : Pd decreases from 4 : 1 to 1 : 1, the total Pd–M CN decreases, while Au–M increases, indicating that Pd is initially predominantly on the surface of the 4 : 1 catalyst and not as predominantly on the surface as the ratio approaches unity. The bond distances listed are in good agreement with the literature[44,51] on bimetallic AuPd systems, with Pd–Pd distances at 2.79 ± 0.01 Å and Au–Au distances of 2.83 ± 0.01 Å. These values are slightly lower than the reference foils, which is typical for NP systems.[102,103]

Compared to the co-reduced samples, slight increases in Pd–Pd CNs become apparent for the sequentially reduced samples. For the seq-Au_4Pd system, a CN of 1.6 ± 0.3 for Pd–Pd and 6.1 ± 0.5 for Pd–Au is observed. As the ratio of Au : Pd decreases, the CN of Pd–Pd increases while Pd–Au decreases, with the seq-AuPd system showing 6.0 ± 0.4 for Pd–Pd, and 3.2 ± 0.6 for Pd–Au. This is a similar trend observed in the co-Au_xPd catalysts. For seq-Au_4Pd, a large CN of 9.5 ± 0.4 for Au–Au is observed. The seq-AuPd catalyst has an Au–Au CN of 11.2 ± 1.1, resembling an Au fcc lattice (CN of 12). This is a sign that all Au atoms are in the interior of the NPs as Au : Pd ratios approach unity. The insignificant Au–Pd interaction for each sequentially-reduced catalyst along with large Pd–Pd and Au–Au interactions would indicate a core–shell morphology rather than an alloy.[24,51,102] Bond distances of ~2.70, ~2.73, and ~2.83 Å for Pd–Pd, Pd–Au, and Au–Au bonds are in good agreement with previous work.[51] The shorter bond distances seen for Pd–Pd and Pd–Au bonds

Table 2 EXAFS fitting parameters for co-Au_xPd catalysts

Catalyst	Bond	CN	*R* (Å)	σ^2 (Å^2)	E_0 (eV)	*R*-Factor
co-Au_4Pd	Pd–Au	8.7 ± 0.8	2.80 ± 0.01	0.008 ± 0.001	−4.1 ± 0.6	0.008
	Pd–Pd	1.2 ± 0.3	2.79 ± 0.02	0.006 ± 0.002	−4.1 ± 0.6	
	Au–Au	7.1 ± 0.7	2.83 ± 0.01	0.009 ± 0.001	4.7 ± 0.4	
	Au–Pd	1.2 ± 0.3	2.80 ± 0.01	0.006 ± 0.002	4.7 ± 0.4	
co-Au_3Pd	Pd–Au	7.2 ± 0.9	2.80 ± 0.01	0.007 ± 0.001	−1.7 ± 0.4	0.016
	Pd–Pd	2.5 ± 0.6	2.79 ± 0.01	0.007 ± 0.002	−1.7 ± 0.4	
	Au–Au	6.3 ± 0.8	2.82 ± 0.01	0.008 ± 0.001	4.2 ± 0.5	
	Au–Pd	1.6 ± 0.3	2.80 ± 0.01	0.004 ± 0.001	4.2 ± 0.5	
co-Au_2Pd	Pd–Au	7.3 ± 0.9	2.80 ± 0.01	0.008 ± 0.002	−5.4 ± 0.4	0.007
	Pd–Pd	2.5 ± 0.4	2.79 ± 0.01	0.005 ± 0.001	−5.4 ± 0.4	
	Au–Au	6.5 ± 1.2	2.82 ± 0.01	0.009 ± 0.002	5.2 ± 0.6	
	Au–Pd	2.7 ± 0.5	2.80 ± 0.01	0.007 ± 0.001	5.2 ± 0.6	
co-AuPd	Pd–Au	6.0 ± 2.4	2.80 ± 0.01	0.008 ± 0.006	−6.2 ± 0.8	0.023
	Pd–Pd	2.4 ± 1.2	2.77 ± 0.03	0.005 ± 0.004	−6.2 ± 0.8	
	Au–Au	5.8 ± 0.9	2.82 ± 0.01	0.008 ± 0.001	6.1 ± 0.6	
	Au–Pd	3.7 ± 0.6	2.80 ± 0.01	0.007 ± 0.001	6.1 ± 0.6	

Table 3 EXAFS fitting parameters for seq-Au_xPd catalysts

Catalyst	Bond	CN	R (Å)	σ^2 (Å^2)	E_0 (eV)	R-Factor
seq-Au_4Pd	Pd–Au	6.1 ± 0.5	2.73 ± 0.01	0.008 ± 0.001	−4.4 ± 0.7	0.017
	Pd–Pd	1.6 ± 0.3	2.68 ± 0.02	0.007 ± 0.002	−4.4 ± 0.7	
	Au–Au	9.5 ± 0.4	2.84 ± 0.01	0.010 ± 0.001	3.5 ± 0.6	
	Au–Pd	ND[a]	ND	ND	ND	
seq-Au_3Pd	Pd–Au	5.2 ± 0.5	2.74 ± 0.01	0.006 ± 0.001	−10.5 ± 0.8	0.020
	Pd–Pd	1.9 ± 0.3	2.69 ± 0.02	0.005 ± 0.002	−10.5 ± 0.8	
	Au–Au	9.5 ± 0.4	2.83 ± 0.01	0.009 ± 0.001	3.0 ± 0.6	
	Au–Pd	0.5 ± 0.1	2.74 ± 0.01	0.004 ± 0.001	3.0 ± 0.6	
seq-Au_2Pd	Pd–Au	5.7 ± 0.7	2.71 ± 0.01	0.011 ± 0.002	−2.9 ± 1.0	0.017
	Pd–Pd	3.3 ± 0.5	2.68 ± 0.02	0.008 ± 0.001	−2.9 ± 1.0	
	Au–Au	12.2 ± 0.7	2.84 ± 0.01	0.011 ± 0.001	4.9 ± 0.7	
	Au–Pd	ND	ND	ND	ND	
seq-AuPd	Pd–Au	3.2 ± 0.6	2.73 ± 0.02	0.008 ± 0.001	−7.6 ± 0.6	0.015
	Pd–Pd	6.0 ± 0.4	2.73 ± 0.01	0.009 ± 0.001	−7.6 ± 0.6	
	Au–Au	11.2 ± 1.1	2.84 ± 0.01	0.009 ± 0.001	4.6 ± 1.2	
	Au–Pd	ND	ND	ND	ND	

[a] ND = not detected. This indicates that the errors in the EXAFS parameter were larger than the value obtained.

(compared to the co-reduced system) are also consistent with phase-separation of the Pd and Au phases, and the lower Pd–Au bond length may be due to lattice mismatches at the Pd–Au interface. Similar to what was seen in the co-reduced system, the seq-Au_4Pd system is the closest to a SAC.

Selective oxidation of crotyl alcohol using co- and seq-reduced Au_xPd catalysts

The co-reduced and sequentially reduced Au_xPd catalysts were monitored for the base-free, room-temperature selective

Table 4 Crotyl alcohol oxidation results[a]

Catalyst	Conversion	Compound	Selectivity	TON	TOF (h^{-1})
co-Au_4Pd	39 ± 9	Crotonaldehyde	77 ± 2	98 ± 22	33 ± 7
		1-Butanol	17 ± 1		
		3-Buten-1-ol	6 ± 3		
co-Au_3Pd	24 ± 2	Crotonaldehyde	65 ± 1	59 ± 4	20 ± 1
		1-Butanol	21 ± 1		
		3-Buten-1-ol	15 ± 1		
co-Au_2Pd	21 ± 3	Crotonaldehyde	67 ± 3	53 ± 8	18 ± 3
		1-Butanol	17 ± 1		
		3-Buten-1-ol	17 ± 1		
co-AuPd	10 ± 1	Crotonaldehyde	36 ± 1	24 ± 2	8 ± 1
		1-Butanol	22 ± 1		
		3-Buten-1-ol	42 ± 1		
seq-Au_4Pd	21 ± 1	Crotonaldehyde	62 ± 1	51 ± 1	17 ± 1
		1-Butanol	20 ± 1		
		3-Buten-1-ol	18 ± 1		
seq-Au_3Pd	15 ± 1	Crotonaldehyde	48 ± 4	37 ± 3	12 ± 1
		1-Butanol	25 ± 2		
		3-Buten-1-ol	27 ± 2		
seq-Au_2Pd	12 ± 1	Crotonaldehyde	35 ± 3	29 ± 2	10 ± 1
		1-Butanol	28 ± 1		
		3-Buten-1-ol	37 ± 2		
seq-AuPd	9 ± 1	Crotonaldehyde	27 ± 2	23 ± 1	8 ± 1
		1-Butanol	29 ± 1		
		3-Buten-1-ol	45 ± 1		
Au NP control[b]	0.3	Crotonaldehyde	0.0	0.8	0.3
		1-Butanol	100.0		
		3-Buten-1-ol	0.0		
Pd NP control[c]	7	Crotonaldehyde	70	17	6
		1-Butanol	22		
		3-Buten-1-ol	8		

[a] All reactions were run for 3 hours, stirring at 1400 rpm at room temperature (22 °C). The Pd : substrate ratio used for all reactions was 1 : 250 (5 mL of sample, 0.32 mL of crotyl alcohol). [Pd] = 3 mM for all Au_xPd catalysts. [b] [Au] = 18.2 mM. [c] [Pd] = 3.0 mM. The average TOF was calculated by dividing the TON by 3 hours.

oxidation of crotyl alcohol to evaluate the selectivity of each catalyst in producing crotonaldehyde. Table 4 shows the results from this reaction with co- and seq-reduced Au_xPd catalysts, as well as monometallic Au and Pd NPs. Both the monometallic NP catalysts showed <10% conversion to the three products of the crotyl alcohol oxidation, crotonaldehyde, 1-butanol, and 3-buten-1-ol. Each bimetallic catalyst was more active (*i.e.*, higher conversion) and more selective to crotonaldehyde than either monometallic catalyst. The pseudo-single-atom co-Au_4Pd catalyst showed the greatest selectivity towards crotonaldehyde formation, at 77%. The largest conversion of 39 ± 9% was also observed for this catalyst. Notably, the selectivity towards crotonaldehyde decreased from the co-Au_4Pd catalyst to the co-AuPd system, which had a selectivity of 36%. This result would suggest that not only is the near SAC system more selective, the selectivity is also related to the minimal Pd–Pd interactions (Table 2) that exist for this catalyst. An increase in side-product formation from the 3 : 1 catalyst down to 1 : 1 would indicate increased amounts of Pd–H species present in the catalyst, which is directly related to the increase in the CNs of Pd–Pd.[51,52] As Pd forms continuous domains on the surface of Au, Pd–H species can be directly adjacent to other Pd catalytic sites, which adsorb the alkene, increasing the likelihood of side-products to form. Comparing the co-reduced catalyst to the sequentially reduced system, a decrease in aldehyde selectivity is observed for the sequentially reduced system at each Au : Pd ratio relative to the co-reduced system. The selectivity to the aldehyde decreases from 62% for seq-Au_4Pd down to 27% for seq-AuPd. Control reactions were performed to show that Au NPs are nearly inert for the oxidation reaction, while Pd NPs show high selectivity, but low conversion. These controls are consistent with previous work.[61] It is interesting to note that the Pd only system, while showing poor activity, does have moderate selectivity towards crotonaldehyde (while addition of Au seems to lower selectivity at lower Au : Pd ratios). We believe this may be due to a secondary, much slower, redox mechanism in which Pd is oxidized on the Pd nanoparticle surface, followed by stoichiometric reactions of Pd(II) salts with crotyl alcohol to give Pd(0) and crotonaldehyde.[104] We have previously shown *via in situ* XAS that this mechanism is not available in bimetallic PdAu systems, as the Pd is tremendously stable to over-oxidation in the bimetallic particles.[51] Turnover numbers (TONs) were generated based on the Pd : substrate ratio in our catalysts, which was 1 : 250, and average turnover frequencies (TOFs) were calculated by dividing the TON by 3 hours. The TON and TOF values can be compared to previous work by Maclennan *et al.*[51] using a seq-$AuPd_3$ catalyst, which used a higher ratio of Pd to Au than our work and different concentrations of each metal ([Pd] = 9.36 mM, [Au] = 3.13 mM). The same Pd : substrate ratio of 1 : 250 was used in this work, as well as similar reaction conditions at ambient temperature (25 °C). In that work, a conversion of 72.4% and selectivity of 62.8% was obtained, with a TON of 180. Our best catalyst, co-Au_4Pd, showed lower conversion (39 ± 9%) and better selectivity (77%). The lower conversion is likely due to the lower Pd concentration used. In this work, we were able to significantly reduce the amount of Pd in the catalyst, while improving the selectivity towards crotonaldehyde. Crotyl alcohol oxidations have also been studied by our group and others, although typically using much harsher reactions (higher *T*, presence of bases) and at lower metal concentrations, which make comparisons difficult.[23,24,61]

A comparison study was performed to show that vinyl acetate (VA) can also be used as a sacrificial alkane to "clean" the surface of the catalyst, similar to how $O_{2(g)}$ removes Pd–H species.[92] This study was done to prove that Pd–H species lead to the production of undesired side-products, and to mitigate side-product formation to drive selectivity towards crotonaldehyde. The result of substituting $O_{2(g)}$ with VA is noted in Table 5. The co-Au_4Pd and co-AuPd catalysts were compared, as well as the seq-Au_4Pd and seq-AuPd catalysts.

Table 5 Crotyl alcohol oxidation results using vinyl acetate[a]

Catalyst	Conversion	Compound	Selectivity	TON	TOF (h^{-1})
co-Au_4Pd	45 ± 1	Crotonaldehyde	88 ± 1	113 ± 2	38 ± 1
		1-Butanol	6.6 ± 0.3		
		3-Buten-1-ol	5.9 ± 0.1		
co-AuPd	17 ± 8	Crotonaldehyde	69 ± 4	42 ± 21	14 ± 7
		1-Butanol	13 ± 2		
		3-Buten-1-ol	18 ± 2		
seq-Au_4Pd	30 ± 1	Crotonaldehyde	78 ± 1	75 ± 1	25 ± 1
		1-Butanol	11 ± 1		
		3-Buten-1-ol	11 ± 1		
seq-AuPd	13 ± 1	Crotonaldehyde	50 ± 1	32 ± 1	11 ± 1
		1-Butanol	20 ± 1		
		3-Buten-1-ol	30 ± 1		
Vinyl acetate	3	Crotonaldehyde	13	6	2
		1-Butanol	80		
		3-Buten-1-ol	7		

[a] All reactions were run for 3 hours, stirring at 1400 rpm at room temperature (22 °C). The Pd : substrate ratio used for all reactions was 1 : 250 (5 mL of sample, 0.32 mL crotyl alcohol), while the substrate : VA ratio was kept at 1 : 1 (0.35 mL VA).

For all four catalysts, increased conversions and selectivities are observed, with the selectivity for the co-Au_4Pd system increasing from 77 ± 2% using $O_{2(g)}$ to 88 ± 1% using VA. Similarly, for seq-Au_4Pd, the selectivity increased from 62 ± 1% to 78 ± 1% using $O_{2(g)}$ and VA, respectively. The reduction of side-product formation would indicate the VA cleans the surface of the catalyst by removing Pd–H species more efficiently than $O_{2(g)}$; this may be due to the fact that VA is in the same phase as the substrate, while O_2 has to diffuse into the liquid phase which sets up possible mass transfer limitations. The significance of using VA is that it is inexpensive, small amounts of it are needed for the oxidation reaction (1 : 1 VA : substrate), and a pressurized system of oxygen gas is not needed. The use of VA also makes it easier to replicate the oxidation reaction, as everything can be thrown into "one-pot" and left to react for a desired amount of time. Additionally, while the use of VA as the oxidant may be impractical due to subsequent issues in separating the products of the reaction, the results show that one of the root causes of poorer selectivity for this reaction when using oxygen as the oxidant is likely caused by mass-transfer challenges of oxygen into the liquid phase.

Conclusions

In conclusion, a series of co- and sequentially-reduced Au_xPd catalysts with x = 4, 3, 2, and 1 were synthesized, characterized, and evaluated as selective catalysts in the oxidation of crotyl alcohol to crotonaldehyde. TEM, XPS, and XAS analysis techniques confirmed that bimetallic co-reduced and seq-reduced Au_xPd nanoparticles were effectively synthesized, with sequentially-reduced Au_xPd nanoparticles showing a core–shell morphology. XPS spectra showed that metallic Au and Pd were present in each catalyst system, and Pd L_{III} edge XAS data showed that Pd was 4d electron deficient in the AuPd systems. Modelling of the EXAFS data confirmed that co-Au_4Pd and seq-Au_4Pd nanoparticles contained nearly isolated Pd atoms (*i.e.* they were pseudo-single-atom catalysts), while other ratios of co- and seq-Au_xPd catalysts showed more contiguous domains of Pd. Results from the oxidation of crotyl alcohol showed that the co-Au_4Pd system was not only more active but also most selective in forming crotonaldehyde. As the ratio of Au : Pd decreased in both co- and seq-Au_xPd catalysts, activity and selectivity decreased. These catalysts were compared to monometallic Au and Pd NPs and were all more active and selective than the monometallic catalysts. Finally, we showed that vinyl acetate could be used as a more effective oxidant in this system which promoted higher selectivity towards crotonaldehyde formation.

Conflicts of interest

There are no conflicts to declare.

Acknowledgements

We would like to thank the National Sciences and Engineering Research Council (NSERC) and the University of Saskatchewan for funding. We would also like to thank Drs. Yongfeng Hu, Qunfeng Xiao, Ning Chen, Weifeng Chen, and Roman Chernikov for their help in collecting XAS data on the SXRMB, HXMA, and BioXAS beamlines. X-ray absorption spectroscopy experiments at the Canadian Light Source, a national research facility of the University of Saskatchewan, which is supported by the Canada Foundation for Innovation (CFI), the Natural Sciences and Engineering Research Council (NSERC), the National Research Council (NRC), the Canadian Institutes of Health Research (CIHR), the Government of Saskatchewan, and the University of Saskatchewan.

Notes and references

1 S. Alayoglu, A. U. Nilekar, M. Mavrikakis and B. Eichhorn, *Nat. Mater.*, 2008, **7**, 333–338.
2 M. Turner, V. B. Golovko, O. P. H. Vaughan, P. Abdulkin, A. Berenguer-Murcia, M. S. Tikhov, B. F. G. Johnson and R. M. Lambert, *Nature*, 2008, **454**, 981–983.
3 D. Wang, A. Villa, P. Spontoni, D. S. Su and L. Prati, *Chem. – Eur. J.*, 2010, **16**, 10007–10013.
4 N. Agarwal, S. J. Freakley, R. U. McVicker, S. M. Althahban, N. Dimitratos, Q. He, D. J. Morgan, R. L. Jenkins, D. J. Willock, S. H. Taylor, C. J. Kiely and G. J. Hutchings, *Science*, 2017, **358**, 223–227.
5 J. Yuan, W. Zhang, X. Li and J. Yang, *Chem. Commun.*, 2018, **54**, 2284–2287.
6 A. W. Petrov, D. Ferri, F. Krumeich, M. Nachtegaal, J. A. van Bokhoven and O. Kröcher, *Nat. Commun.*, 2018, **9**, 2545.
7 J. M. Thomas, B. F. G. Johnson, R. Raja, G. Sankar and P. A. Midgley, *Acc. Chem. Res.*, 2003, **36**, 20–30.
8 J. Liu, J. Shan, F. R. Lucci, S. Cao, E. C. H. Sykes and M. Flytzani-Stephanopoulos, *Catal. Sci. Technol.*, 2017, **7**, 4276–4284.
9 L. B. Okhlopkova, S. V. Cherepanova, I. P. Prosvirin, M. A. Kerzhentsev and Z. R. Ismagilov, *Appl. Catal., A*, 2018, **549**, 245–253.
10 L. B. Okhlopkova, M. A. Kerzhentsev and Z. R. Ismagilov, *Kinet. Catal.*, 2018, **59**, 450–458.
11 S. Kattel, P. J. Ramírez, J. G. Chen, J. A. Rodriguez and P. Liu, *Science*, 2017, **355**, 1296–1299.
12 F. Huang, Y. Deng, Y. Chen, X. Cai, M. Peng, Z. Jia, P. Ren, D. Xiao, X. Wen, N. Wang, H. Liu and D. Ma, *J. Am. Chem. Soc.*, 2018, **140**, 13142–13146.
13 D. Astruc, F. Lu and J. R. Aranzaes, *Angew. Chem., Int. Ed.*, 2005, **44**, 7852–7872.
14 S. K. Beaumont, *J. Chem. Technol. Biotechnol.*, 2012, **87**, 595–600.
15 S. Sawoo, D. Srimani, P. Dutta, R. Lahiri and A. Sarkar, *Tetrahedron*, 2009, **65**, 4367–4374.
16 H. Zhang, G. Liu, L. Shi and J. Ye, *Adv. Energy Mater.*, 2018, **8**, 1701343.

17 X.-F. Yang, A. Wang, B. Qiao, J. Li, J. Liu and T. Zhang, *Acc. Chem. Res.*, 2013, **46**, 1740–1748.
18 S. Liang, C. Hao and Y. Shi, *ChemCatChem*, 2015, **7**, 2559–2567.
19 M. Dhiman and V. Polshettiwar, *ChemCatChem*, 2018, **10**, 881–906.
20 Z. Chen, E. Vorobyeva, S. Mitchell, E. Fako, N. López, S. M. Collins, R. K. Leary, P. A. Midgley, R. Hauert and J. Pérez-Ramírez, *Natl. Sci. Rev.*, 2018, **5**, 642–652.
21 S. Mitchell, E. Vorobyeva and J. Pérez-Ramírez, *Angew. Chem., Int. Ed.*, 2018, **57**, 15316–15329.
22 J. Kim, H.-E. Kim and H. Lee, *ChemSusChem*, 2018, **11**, 104–113.
23 W. Hou, N. A. Dehm and R. W. J. Scott, *J. Catal.*, 2008, **253**, 22–27.
24 T. Balcha, J. R. Strobl, C. Fowler, P. Dash and R. W. J. Scott, *ACS Catal.*, 2011, **1**, 425–436.
25 S. Hayashi, R. Ishida, S. Hasegawa, S. Yamazoe and T. Tsukuda, *Top. Catal.*, 2018, **61**, 136–141.
26 Y. Chen, F. Yang, Y. Dai, W. Wang and S. Chen, *J. Phys. Chem. C*, 2008, **112**, 1645–1649.
27 Z. Chen, S. Mitchell, E. Vorobyeva, R. K. Leary, R. Hauert, T. Furnival, Q. M. Ramasse, J. M. Thomas, P. A. Midgley, D. Dontsova, M. Antonietti, S. Pogodin, N. López and J. Pérez-Ramírez, *Adv. Funct. Mater.*, 2017, **27**, 1605785.
28 P. Xin, J. Li, Y. Xiong, X. Wu, J. Dong, W. Chen, Y. Wang, L. Gu, J. Luo, H. Rong, C. Chen, Q. Peng, D. Wang and Y. Li, *Angew. Chem., Int. Ed.*, 2018, **57**, 4642–4646.
29 X. Huang, H. Yan, L. Huang, X. Zhang, Y. Lin, J. Li, Y. Xia, Y. Ma, Z. Sun, S. Wei and J. Lu, *J. Phys. Chem. C*, 2019, **123**, 7922–7930.
30 G. Gao, Y. Jiao, E. R. Waclawik and A. Du, *J. Am. Chem. Soc.*, 2016, **138**, 6292–6297.
31 B. Zhang, G. Sun, S. Ding, H. Asakura, J. Zhang, P. Sautet and N. Yan, *J. Am. Chem. Soc.*, 2019, **141**, 8185–8197.
32 F. R. Lucci, J. Liu, M. D. Marcinkowski, M. Yang, L. F. Allard, M. Flytzani-Stephanopoulos and E. C. H. Sykes, *Nat. Commun.*, 2015, **6**, 8550.
33 J. Liu, F. R. Lucci, M. Yang, S. Lee, M. D. Marcinkowski, A. J. Therrien, C. T. Williams, E. C. H. Sykes and M. Flytzani-Stephanopoulos, *J. Am. Chem. Soc.*, 2016, **138**, 6396–6399.
34 M. Yang, L. F. Allard and M. Flytzani-Stephanopoulos, *J. Am. Chem. Soc.*, 2013, **135**, 3768–3771.
35 J. Lin, A. Wang, B. Qiao, X. Liu, X. Yang, X. Wang, J. Liang, J. Li, J. Liu and T. Zhang, *J. Am. Chem. Soc.*, 2013, **135**, 15314–15317.
36 R. Lang, T. Li, D. Matsumura, S. Miao, Y. Ren, Y.-T. Cui, Y. Tan, B. Qiao, L. Li, A. Wang, X. Wang and T. Zhang, *Angew. Chem., Int. Ed.*, 2016, **55**, 16054–16058.
37 L. Liu, X. Wu, L. Wang, X. Xu, L. Gan, Z. Si, J. Li, Q. Zhang, Y. Liu, Y. Zhao, R. Ran, X. Wu, D. Weng and F. Kang, *Commun. Chem.*, 2019, **2**, 18.
38 H.-E. Kim, I. H. Lee, J. Cho, S. Shin, H. C. Ham, J. Y. Kim and H. Lee, *ChemElectroChem*, 2019, **6**, 4757–4764.
39 M. J. Hülsey, J. Zhang and N. Yan, *Adv. Mater.*, 2018, **30**, 1802304.
40 Y. Sun, J. Zhou, H. Ji, J. Liu, T. Qian and C. Yan, *ACS Appl. Mater. Interfaces*, 2019, **11**, 32008–32014.
41 D. Deng, X. Chen, L. Yu, X. Wu, Q. Liu, Y. Liu, H. Yang, H. Tian, Y. Hu, P. Du, R. Si, J. Wang, X. Cui, H. Li, J. Xiao, T. Xu, J. Deng, F. Yang, P. N. Duchesne, P. Zhang, J. Zhou, L. Sun, J. Li, X. Pan and X. Bao, *Sci. Adv.*, 2015, **1**, e1500462.
42 H. Zhang, J. Wei, J. Dong, G. Liu, L. Shi, P. An, G. Zhao, J. Kong, X. Wang, X. Meng, J. Zhang and J. Ye, *Angew. Chem., Int. Ed.*, 2016, **55**, 14310–14314.
43 G. S. Parkinson, *Catal. Lett.*, 2019, **149**, 1137–1146.
44 C. J. Wrasman, A. Boubnov, A. R. Riscoe, A. S. Hoffman, S. R. Bare and M. Cargnello, *J. Am. Chem. Soc.*, 2018, **140**, 12930–12939.
45 X. Zhu, Q. Guo, Y. Sun, S. Chen, J.-Q. Wang, M. Wu, W. Fu, Y. Tang, X. Duan, D. Chen and Y. Wan, *Nat. Commun.*, 2019, **10**, 1428.
46 G. Giannakakis, M. Flytzani-Stephanopoulos and E. C. H. Sykes, *Acc. Chem. Res.*, 2019, **52**, 237–247.
47 Y. Pan, K. Sun, S. Liu, X. Cao, K. Wu, W.-C. Cheong, Z. Chen, Y. Wang, Y. Li, Y. Liu, D. Wang, Q. Peng, C. Chen and Y. Li, *J. Am. Chem. Soc.*, 2018, **140**, 2610–2618.
48 M. Newville, *Rev. Mineral. Geochem.*, 2014, **78**, 33–74.
49 J. Yano and V. K. Yachandra, *Photosynth. Res.*, 2009, **102**, 241–254.
50 G. Bunker, *Introduction to XAFS*, Cambridge University Press, Cambridge, U.K., 2011.
51 A. Maclennan, A. Banerjee, Y. Hu, J. T. Miller and R. W. J. Scott, *ACS Catal.*, 2013, **3**, 1411–1419.
52 A. Maclennan, A. Banerjee and R. W. J. Scott, *Catal. Today*, 2013, **207**, 170–179.
53 J. Liu, M. B. Uhlman, M. M. Montemore, A. Trimpalis, G. Giannakakis, J. Shan, S. Cao, R. T. Hannagan, E. C. H. Sykes and M. Flytzani-Stephanopoulos, *ACS Catal.*, 2019, **9**, 8757–8765.
54 H. Zhou, S. Hong, H. Zhang, Y. Chen, H. Xu, X. Wang, Z. Jiang, S. Chen and Y. Liu, *Appl. Catal., B*, 2019, **256**, 117767.
55 J. Zhao, R. Qin and R. Liu, *Appl. Catal., B*, 2019, **256**, 117778.
56 A. Shivhare and R. W. J. Scott, *J. Mol. Catal.*, 2018, **457**, 33–40.
57 V. Sudheeshkumar, A. Shivhare and R. W. J. Scott, *Catal. Sci. Technol.*, 2017, **7**, 272–280.
58 E.-K. Lee, S.-A. Park, H. Woo, K. Hyun Park, D. W. Kang, H. Lim and Y.-T. Kim, *J. Catal.*, 2017, **352**, 388–393.
59 J. Li, Y. Xu, S. Wang and H. Zhang, *J. Phys. Chem. C*, 2019, **123**, 15483–15494.
60 L. Abis, N. Dimitritatos, M. Sankar, S. J. Freakley and G. J. Hutchings, *Catal. Sci. Technol.*, 2019, **9**, 5686–5691.
61 K. E. Lee, A. Shivhare, Y. Hu and R. W. J. Scott, *Catal. Today*, 2017, **280**, 259–265.
62 N. Hayashi, Y. Sakai, H. Tsunoyama and A. Nakajima, *Langmuir*, 2014, **30**, 10539–10547.
63 L. Prati, A. Villa, C. E. Chan-Thaw, R. Arrigo, D. Wang and D. S. Su, *Faraday Discuss.*, 2011, **152**, 353–365.
64 P. Miedziak, M. Sankar, N. Dimitratos, J. A. Lopez-Sanchez, A. F. Carley, D. W. Knight, S. H. Taylor, C. J. Kiely and G. J. Hutchings, *Catal. Today*, 2011, **164**, 315–319.

65 A. F. Lee, C. V. Ellis, J. N. Naughton, M. A. Newton, C. M. A. Parlett and K. Wilson, *J. Am. Chem. Soc.*, 2011, **133**, 5724–5727.
66 N. Dimitratos, J. A. Lopez-Sanchez and G. J. Hutchings, *Chem. Sci.*, 2011, **3**, 20–44.
67 A. J. Frank, J. Rawski, K. E. Maly and V. Kitaev, *Green Chem.*, 2010, **12**, 1615–1622.
68 A. Villa, N. Janjic, P. Spontoni, D. Wang, D. S. Su and L. Prati, *Appl. Catal., A*, 2009, **364**, 221–228.
69 P. G. N. Mertens, S. L. F. Corthals, X. Ye, H. Poelman, P. A. Jacobs, B. F. Sels, I. F. J. Vankelecom and D. E. De Vos, *J. Mol. Catal. A: Chem.*, 2009, **313**, 14–21.
70 D. I. Enache, J. K. Edwards, P. Landon, B. Solsona-Espriu, A. F. Carley, A. A. Herzing, M. Watanabe, C. J. Kiely, D. W. Knight and G. J. Hutchings, *Science*, 2006, **311**, 362–365.
71 C. Williams, J. H. Carter, N. F. Dummer, Y. K. Chow, D. J. Morgan, S. Yacob, P. Serna, D. J. Willock, R. J. Meyer, S. H. Taylor and G. J. Hutchings, *ACS Catal.*, 2018, **8**, 2567–2576.
72 J. Jover, M. García-Ratés and N. López, *ACS Catal.*, 2016, **6**, 4135–4143.
73 A. F. Lee, C. V. Ellis, K. Wilson and N. S. Hondow, *Catal. Today*, 2010, **157**, 243–249.
74 K. Mori, T. Hara, T. Mizugaki, K. Ebitani and K. Kaneda, *J. Am. Chem. Soc.*, 2004, **126**, 10657–10666.
75 Y. Feng, L. Zhou, Q. Wan, S. Lin and H. Guo, *Chem. Sci.*, 2018, **9**, 5890–5896.
76 N. Toshima and T. Yonezawa, *New J. Chem.*, 1998, **22**, 1179–1201.
77 M. Harada, K. Asakura and N. Toshima, *J. Phys. Chem.*, 1993, **97**, 5103–5114.
78 J. H. Sinfelt, *Acc. Chem. Res.*, 1977, **10**, 15–20.
79 K. Zhao, Y. Zhu, J. Shi, X. Zhao, R. Pang, X. Xue, X. Ren, X. Duan, Z. X. Guo and S. Li, *J. Mater. Chem. A*, 2019, **7**, 9297–9304.
80 L. Zhang, A. Wang, W. Wang, Y. Huang, X. Liu, S. Miao, J. Liu and T. Zhang, *ACS Catal.*, 2015, **5**, 6563–6572.
81 R. Réocreux, M. Uhlman, T. Thuening, P. Kress, R. Hannagan, M. Stamatakis and E. C. H. Sykes, *Chem. Commun.*, 2019, **55**, 15085–15088.
82 B. Xu, H. Wang, W. Wang, L. Gao, S. Li, X. Pan, H. Wang, H. Yang, X. Meng, Q. Wu, L. Zheng, S. Chen, X. Shi, K. Fan, X. Yan and H. Liu, *Angew. Chem., Int. Ed.*, 2019, **58**, 4911–4916.
83 T. Sharifi, E. Gracia-Espino, A. Chen, G. Hu and T. Wågberg, *Adv. Energy Mater.*, 2020, **10**, 1902084.
84 M. Chen and C. Chen, *Angew. Chem., Int. Ed.*, 2018, **57**, 3094–3098.
85 G. X. Pei, X. Y. Liu, A. Wang, L. Li, Y. Huang, T. Zhang, J. W. Lee, B. W. L. Jang and C.-Y. Mou, *New J. Chem.*, 2014, **38**, 2043–2051.
86 G. Vilé, D. Albani, M. Nachtegaal, Z. Chen, D. Dontsova, M. Antonietti, N. López and J. Pérez-Ramírez, *Angew. Chem., Int. Ed.*, 2015, **54**, 11265–11269.
87 H. Tsunoyama, N. Ichikuni and T. Tsukuda, *Langmuir*, 2008, **24**, 11327–11330.
88 W. S. Rasband, ImageJ, https://imagej.nih.gov/ij/.
89 N. Fairley, Copyright © 2005 Casa Software Ltd., http://www.casaxps.com/.
90 J. Shen, R. W. J. Scott, R. E. Hayes and N. Semagina, *Appl. Catal., A*, 2015, **502**, 350–360.
91 M. Newville, *J. Synchrotron Radiat.*, 2001, **8**, 322–324.
92 J. Muzart, *Tetrahedron*, 2003, **59**, 5789–5816.
93 R. W. J. Scott, O. M. Wilson, S.-K. Oh, E. A. Kenik and R. M. Crooks, *J. Am. Chem. Soc.*, 2004, **126**, 15583–15591.
94 M.-C. Daniel and D. Astruc, *Chem. Rev.*, 2004, **104**, 293–346.
95 J. F. Moulder, W. F. Stickle, P. E. Sobol and K. D. Bomben, *Handbook of X-ray Photoelectron Spectroscopy*, Perkin-Elmer Corp, Eden Prairie, MN, 1992.
96 A. van Triest, W. Folkerts and C. Haas, *J. Phys.: Condens. Matter*, 1990, **2**, 8733–8740.
97 L. C. Witjens, J. H. Bitter, A. J. van Dillen, K. P. de Jong and F. M. F. de Groot, *Phys. Chem. Chem. Phys.*, 2004, **6**, 3903–3906.
98 G. Meitzner and J. H. Sinfelt, *Catal. Lett.*, 1994, **30**, 1–10.
99 D. C. Huang, K. H. Chang, W. F. Pong, P. K. Tseng, K. J. Hung and W. F. Huang, *Catal. Lett.*, 1998, **53**, 155–159.
100 C. Liu, N. Chen, J. Li, X. Gao, T.-K. Sham and S.-D. Wang, *J. Phys. Chem. C*, 2017, **121**, 28385–28394.
101 L. Zhang, A. Wang, J. T. Miller, X. Liu, X. Yang, W. Wang, L. Li, Y. Huang, C.-Y. Mou and T. Zhang, *ACS Catal.*, 2014, **4**, 1546–1553.
102 F. Liu, D. Wechsler and P. Zhang, *Chem. Phys. Lett.*, 2008, **461**, 254–259.
103 S. L. Christensen, A. Chatt and P. Zhang, *Langmuir*, 2012, **28**, 2979–2985.
104 K. Zaw, M. Lautens and P. M. Henry, *Organometallics*, 1983, **2**, 197–199.